Lasers in Dermatology

R. Steiner R. Kaufmann M. Landthaler
O. Braun-Falco (Eds.)

Lasers in Dermatology

Proceedings of the International Symposium,
Ulm, 26 September 1989

With 59 Figures

Springer-Verlag
Berlin Heidelberg New York
London Paris Tokyo
Hong Kong Barcelona
Budapest

Professor Dr. Rudolf Steiner
Institut für Lasertechnologien in der Medizin an der Universität Ulm, Postfach 4066,
Helmholtzstrasse 12, W-7900 Ulm, Fed. Rep. of Germany

Priv.-Doz. Dr. med. Roland Kaufmann
Dermatologische Klinik der Universität Ulm, Oberer Eselsberg 40,
W-7900 Ulm, Fed. Rep. of Germany

Prof. Dr. med. Michael Landthaler
Prof. Dr. med. Dr. h. c. mult. Otto Braun-Falco
Dermatologische Klinik und Poliklinik der Ludwig-Maximilians-Universität München,
Frauenlobstrasse 9–11, W-8000 München 2, Fed. Rep. of Germany

ISBN 3-540-51863-0 Springer-Verlag Berlin Heidelberg New York
ISBN 0-387-51863-0 Springer-Verlag New York Berlin Heidelberg

Printed in Germany

56/3140-543210 – Printed on acid-free paper

Preface

Therapeutic laser applications in dermatology have become increasingly important during the last ten years. There are indications such as portwine stain lesions where only the laser (argon or dye) can produce satisfying results. The other "classic" types of laser (CO_2 and Nd:YAG) are widely used for outpatient treatment. Tissue removal or tissue coagulation are the two forms of either thermal or ablative laser–tissue interaction. Fundamental research work has led to a comprehensive understanding of light distribution in skin and other biological tissues. Understanding the optical properties of a tissue, such as reflectance and transmittance, is the first step towards predicting the best therapy. In addition, the laser parameters wavelength, energy and pulse duration modulate the tissue reactions, thus influencing the therapeutic result.

This book is a notable summary of the state of the art of lasers in dermatology. Starting with the basic theory of laser–tissue interaction and continuing with routine laser applications, this book also includes reports on new types of laser and their possible therapeutic potential. Future aspects of lasers in dermatology will concentrate mainly on pulsed laser techniques from the ultraviolet part of the spectrum to the infrared. The advantage of frequency doubling of the laser light and its effect on tissue reactions is also discussed.

Physicians, and especially dermatologists, working in the field of laser applications will profit from this book, gaining a deeper understanding of the process of laser interaction with tissue and being therefore able to improve their techniques and methods of laser application. For newcomers this book is also the ideal introduction to all the possible and established uses of the different types of laser for the maximum benefit of patients.

Ulm,
December 1990

R. Steiner
R. Kaufmann
M. Landthaler
O. Braun-Falco

Contents

The Role of Skin Optics in Diagnostic and Therapeutic Uses of Lasers
By S.L. Jacques (With 10 Figures) 1

Photodynamic Therapy in the Treatment of Diseases of the Skin
By J.A.S. Carruth and S.R. Williams 22

The CO_2 Laser in Dermatotherapy
By M. Landthaler and U. Hohenleutner (With 1 Figure) 26

The Argon Laser in Dermatotherapy
By M. Landthaler, U. Hohenleutner, G. Donhauser, and O. Braun-Falco
(With 5 Figures) 44

Dye Laser for Benign Cutaneous Vascular Lesions:
Clinical and Technical Development
By O.T. Tan (With 5 Figures) 60

The Neodymium YAG Laser in Dermatology
By F.A. Bahmer (With 7 Figures) 73

Treatment of Deep Located Haemangiomas
with the Nd:YAG Laser (1064 nm)
By C. Philipp, H.P. Berlien, and J. Waldschmidt (With 2 Figures) 85

Argon Laser Treatment of Port-Wine Stains and Quantitative Evaluation
by Reflected Subject Color Analysis
By R.A. Neumann, R.M. Knobler, and A. Lindmaier (With 3 Figures) . . 91

Fundamentals of Pulsed UV and Mid-infrared Laser Skin Ablation
By R. Hibst and R. Kaufmann (With 9 Figures) 102

The ArF Excimer Laser in Dermatology
By S.L. Jacques (With 6 Figures) 116

Pulsed UV and Mid-infrared Laser Skin Ablation:
Experimental and First Clinical Results
By R. Kaufmann and R. Hibst (With 7 Figures) 130

The Short Pulse Dye Laser in the Treatment of Port-Wine Stains
By H. Strempel (With 4 Figures) 147

Future Aspects of Lasers in Dermatology
By R. Steiner 154

Index of Contributors 159

The Role of Skin Optics in Diagnostic and Therapeutic Uses of Lasers

S.L. Jacques

Laser Biology Research Laboratory, University of Texas,
M.D. Anderson Cancer Center – 17, 1515 Holcombe Blvd.
Houston, TX 77030, USA

1. Introduction

Light must penetrate the skin before it can exert therapeutic effect or offer diagnostic information. Laser radiation will penetrate some tissues better than others due to variation in tissue optical properties. Skin is a particularly difficult tissue to penetrate because of the strong scattering properties of the dermis. Fortunately, skin is a relatively thin tissue, and the shallow penetration of light is sufficient for strong interaction with the epidermis and upper dermis. The availability of the skin surface for topical irradiation makes the use of lasers in dermatology an attractive modality.

This paper will discuss the basics of skin optics that are pertinent to proper dosimetry of laser irradiation in dermatology. Examples of dosimetry for wavelengths pertinent to photodynamic therapy and for laser therapy of portwine stain lesions at 577-nm wavelength are presented.

2. Tissue optical properties

2.1 Clinical perspective

The movement of photons through a tissue is determined by the *intrinsic* optical properties of the tissue: the absorption coefficient, μ_a, the scattering coefficient, μ_s, and the anisotropy of scattering, g. In contrast to intrinsic properties, *observable parameters* such as reflectance (R), transmittance (T), and the internal light distribution (ϕ) will change with geometrical factors such as tissue thickness, surface boundary conditions (eg., air/tissue versus water/tissue), and angle of incident irradiation, despite constant instrinsic optical properties. Understanding the optical properties of a tissue is the first step toward comprehensive understanding of laser dosimetry for a variety of delivery conditions.

For example, consider a freshly peeled potato. Slice a thin layer from the potato, and irradiate both the thin slice and the whole potato with light. The R, T, and ϕ for the slice and the whole potato will differ, although both have the same optical properties. The geometrical factor of potato thickness influences the observable parameters despite constant optical properties.

We deduce the optical properties from observable parameters such as R and T under carefully controlled geometric conditions (flat thin slab). Then we use the optical

Lasers in Dermatology
Editors: R. Steiner · R. Kaufmann · M. Landthaler · O. Braun-Falco

properties to predict laser dosimetry in terms of light (ϕ, W/cm^2) or heat ($\mu_a\phi$, W/cm^3) for a particular geometric situation (laser delivery, tissue size and shape, boundary conditions) that is pertinent to a clinical protocol.

2.2 Absorption coefficient, μ_a

The absorption coefficient (μ_a) is defined as the incremental loss of radiant fluence rate (ϕ) that occurs over a unit of pathlength (L): $\mu_a = -d\phi/dL$. In simple terms, μ_a specifies the transmission (T) without absorption over a pathlength (L), expressed as: $T = \exp(-\mu_a L)$. The mean free path, mfp, between absorption events is $1/\mu_a$, and if L equals the mfp then transmission equals 37%. For example, a typical μ_a value for bloodless dermis at the yellow 577-nm wavelength is 2 cm^{-1}, and the mfp is 1/2 cm, or 5 mm. After an ensemble of photons has traveled 5 mm, only 37% of the photons remain unabsorbed and 63% of the photons have been absorbed. Note that the pathlength L need not be in a straight line. Many scattering events may deflect each photon many times. The pathlength L refers to the total path traveled by a photon regardless of directional changes due to scattering.

2.3 Scattering coefficient, μ_s

The scattering coefficient, μ_s, specifies the transmission T without scattering over a path L, expressed as: $T = \exp(-\mu_s L)$. The mfp between scattering events is $1/\mu_s$. For example, a typical μ_s value for bloodless dermis at the yellow 577-nm wavelength is 200 cm^{-1}, and the mfp is 1/200 cm, or 50 μm. Compared to the mfp between absorption events, 5 mm, the occurence of scattering events is quite frequent in the dermis for yellow light. On the average at the yellow 577-nm wavelength, there are 100 scattering events before an absorption event finally occurs.

2.4 Anisotropy of scattering, g

When a photon is scattered, the direction of photon deflection must be considered. The anisotropy, g, describes the average angle, θ, of deflection when a scattering event occurs. The g is defined as the average value of the cosine of the angle of deflection: $g = \langle\cos\theta\rangle$. The definition of g is discussed more fully in the next paragraph, but first let us consider the basic importance of anisotropy. If the deflection angle is totally random (isotropic scattering, g = 0) in a medium, then a single scattering event will cause a photon to lose any sense of its initial direction of delivery to the medium, and the photon will participate in a random walk within the media with mean free steps of $1/\mu_s$ between scattering events. In tissues however, the deflection angle is usually slight (eg., θ between 5° to 45°) and the photon continues its trajectory in the forward direction with only a small deflection. The photon will require approximately 1/(1-g) scattering events before it loses any sense of its initial direction of delivery to the tissue, and the photon will then propagate as a random walk with mean free steps of $1/(\mu_s(1-g))$. For example, yellow light at 577-nm wavelength has a g value of about 0.8 for dermis. Note that the cos(37°) equals 0.8, and

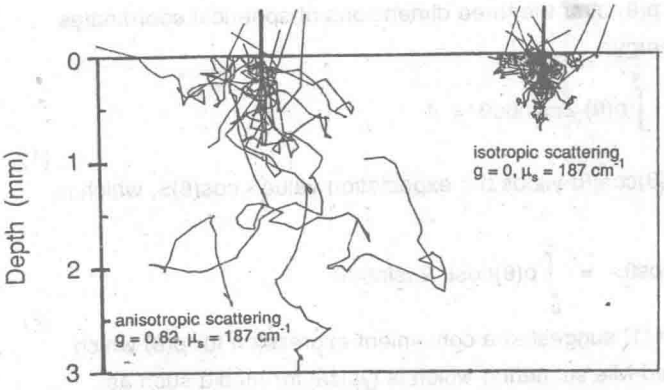

Figure 1: Propagation of photons in human dermis.
(Left) The trajectories of 25 photons at 633-nm wavelength are charted by Monte Carlo simulation, using the optical properties of bloodless dermis: $\mu_a = 2.7\ cm^{-1}$, $\mu_s = 187\ cm^{-1}$, and g = 0.82. **(Right)** The trajectories of 25 photons in an isotropically scattering media (g = 0) with the same μ_a and μ_s values. The figure illustrates how the forward-directed nature of scattering in dermis allows deep penetration of photons into dermis. The trajectories terminate when an absorption event occurs.

the average equivalent θ is ~37°. The photon requires 1/(1-0.8) or 5 scattering events before achieving a random walk. Since the mfp between scattering events is 50 μm, the photon travels 250 μm before its propagation is truly a random walk. Each photon still has 95 (= 100 - 5) scattering events, or 4.75 mm (= 5 mm - 250 μm) of travel before there is a 63% probability of absorption. Therefore, most of the photon's life is spent in random walk.

The size of the mean free steps in the photon's random walk is very important in determing the lateral spread and deep penetration of a laser beam into skin. The mean free steps for tissue equal $1/(\mu_s(1-g))$, but if g equals zero the steps are only $1/\mu_s$. In our example of skin at 577-nm wavelength, the steps are 250 μm because g = 0.8, but if the scattering were isotropic (g = 0) then the steps would be only 50-μm steps. The forward-directed nature of scattering in skin yields large equivalent steps in the photon's random walk. These larger steps allow photons to diffuse further in skin than in an isotropically scattering media of equal μ_s before a given amount of photon absorption occurs.

Figure 1 illustrates the propagation of 25 photons (633 nm, HeNe laser) in human dermis (g = 0.82), and for an equivalent isotropically scattering tissue (g = 0). In both cases, the absorption (μ_a) and scattering (μ_s) coefficients are 2.7 and 187 cm^{-1}, respectively. Note how the isotropic scattering causes photons to remain near the point of entry, but the anisotropic scattering characteristic of dermis allows photon to propagate much deeper into tissue.

For a moment, let us discuss more carefully the concept of anisotropy. When photons are scattered, the distribution of the deflection angle, θ, is conventionally described by a probability distribution function, p(θ), as observed in a single plane of

observation. The integration of p(θ) over the three dimensions of spherical coordinates must equal unity to conserve energy:

$$\int_0^{\pi} p(\theta)\, 2\pi \sin\theta d\theta = 1 \qquad (1)$$

The integration of the product p(θ)cos(θ) yields the expectation value <cos(θ)>, which is the definition of g:

$$g \equiv \langle \cos\theta \rangle = \int_0^{\pi} p(\theta)\cos\theta\, 2\pi \sin\theta d\theta \qquad (2)$$

In 1941, Henyey and Greenstein [1] suggested a convenient expression for p(θ) which approximates the forward-directed Mie scattering which is typical for media such as galaxies or biological tissue [2] whose particles or scattering structures have a size that is similar to the photon wavelength:

$$p_{HG}(\theta) = \frac{1 - g_{HG}^2}{(1 + g_{HG}^2 - 2g_{HG}\cos\theta)^{3/2}} \qquad (3)$$

If this $p_{HG}(\theta)$ is substituted for p(θ) in eq. 2, the g value calculated by eq. 2 will equal the g_{HG} of eq. 3. Henyey and Greenstein were rather clever.

For example, consider the angular scattering of red light (633 nm, HeNe laser) in human dermis. Jacques et al [2] showed that on the average 90% of photons were scattered as a Henyey-Greenstein function with $g_{HG} = 0.91$, and 10% were scattered isotropically, $g_{isotropic} = 0$. The overall g value is equal to the product $g_{HG}(90\%)$, or 0.82 (illustrated in Fig. 1). The authors used alternative experiments (integrating sphere and collimated transmission experiments, see below) to specify an effective g value of 0.81, which agreed with the 0.82 value from angular scattering experiments.

3. Measurement of tissue optical properties

3.1 Clinical perspective

Now that the optical properties are defined, let us consider how optical properties are measured. Generating such information is normally not the task of the laser clinician. Therefore, this chapter simply provides background on how optical properties are specified experimentally in the laboratory.

Skin is particularly heterogeneous, and therefore optically complicated. The pigmented epidermis, the nonpigmented dermis, and the dermal blood vessels constitute a challenge to optical modeling. Heterogeneous skin optics will be discussed in section 4. At this time, we will discuss the optical properties of three component tissue types: (1) pigmented epidermis, (2) bloodless dermis, and (3) blood.

3.2 Dermal optical properties

Two experimental techniques will be presented in this section, total attenuation and integrating sphere measurements, which are generally applicable to studies of tissue optical properties. The work of three students who conducted experiments with this author are presented: Scott Prahl (University of Texas at Austin, A. J. Welch advisor), David Zrakit (Massachusetts Institute of Technology), and Craig Alter (Harvard Medical School). Their work has been published elsewhere as cited. For these experiments on dermis, the epidermis was removed from the dermis by mild heat treatment at 55°C for two minutes in a water bath. Dermal samples were soaked in saline to provide a stable hydration of about 85% water content (g water/g total). Normally, *in vivo* human dermis is closer to 65-70% water content, and therefore the data only approximate *in vivo* optical properties. More work on skin optics is still need.

3.2.1 Total attenuation measurements

The attenuation of a primary laser is due to both absorption and scattering. If a narrow collimated beam is passed through a very thin tissue slab of thickness d, then the transmission of the collimated beam that is collected by a distant narrow aperture detector is given:

$$T_{collimated} = e^{-(\mu_a + \mu_s)d} \tag{4}$$

Tissue sample is held between glass slides during measurements, and thickness is measured by micrometer. The sum of absorption and scattering, $(\mu_a + \mu_s)$, can be specified:

$$\mu_a + \mu_s = \frac{-\ln(T_{collimated})}{d} \tag{5}$$

Usually $\mu_s >> \mu_a$, therefore the total attenuation measurement is principally a measure of μ_s.

Such an experiment is illustrated schematically in Fig. 2a. The samples must be very thin (typically ≤100 μm) to allow sufficient unscattered, unabsorbed light to pass for detection. The solid angle of collection by the detector must be sufficiently small to reject even slightly deflected photons. For example, a 2-mm diameter aperture at a distance of 15 cm from the tissue sample collected a solid angle of 10^{-4} steradians.

Zrakit [3] and Prahl [4] both used a spectrophotometer with narrow apertures to conduct the measurements over the entire UV and visible spectrum. Jacques et al. [2] used a collimated HeNe laser beam to conduct the measurement at 633 nm. Both methods collected a solid angle of ~10^{-4} sr. Figure 2c illustrates a typical spectrum of $T_{collimated}$ through a 360-μm thickness of bloodless dermis, data redrawn from Prahl [4].

3.2.2 Integrating sphere measurements

An integrating sphere (Fig. 2b) is a device which allows collection of light despite scattering. It is used to make measurements of the total transmission, T_t, and the total reflectance, R_t, from a slab of tissue. The tissue sample is usually rather thick (200-1000 μm) and therefore transmission consists of multiply scattered photons. The total

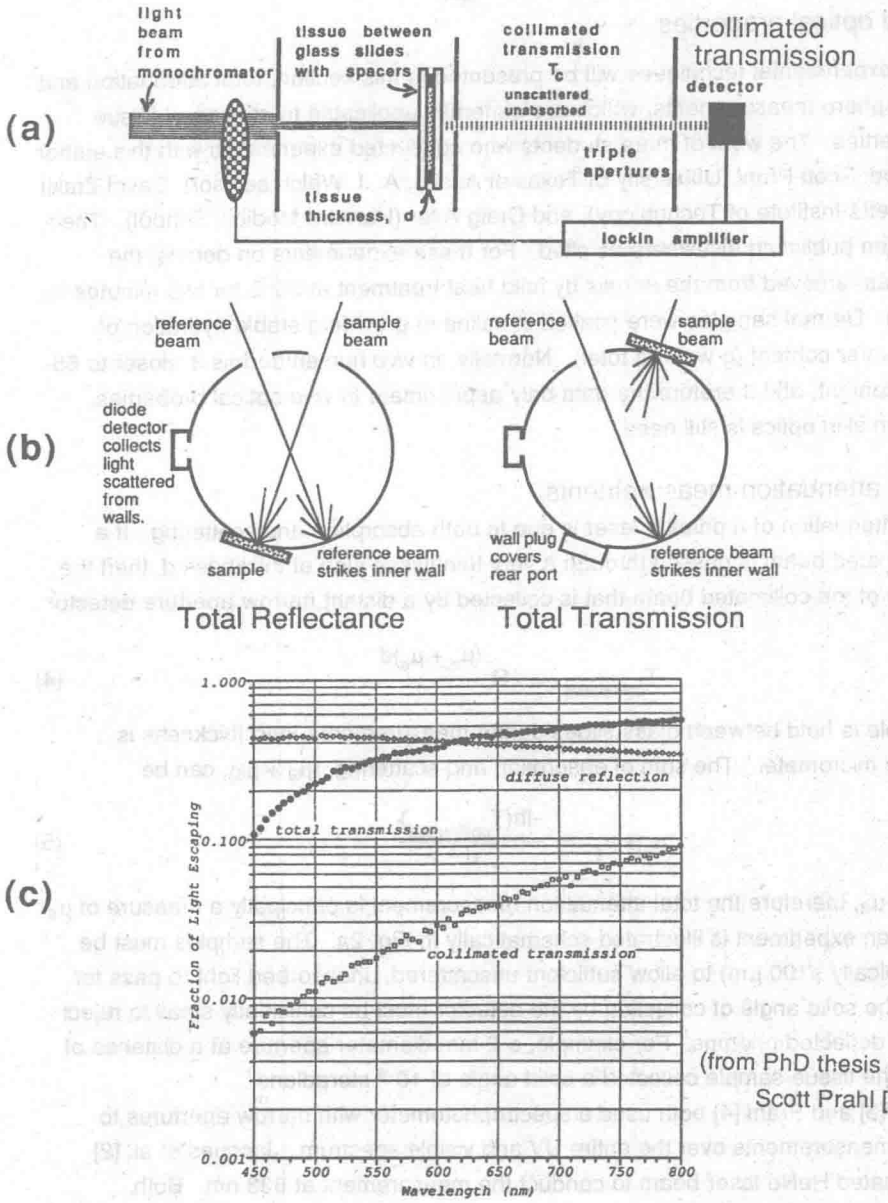

Figure 2: Optical measurements of bloodless dermis.
(a) Total attenuation experiments measure the attenuation of a narrow beam by both absorption and scattering in a thin sample (≤100 μm thickness). **(b)** Integrating sphere experiments measure the total transmission (T_t) and total reflectance (R_t) from a thick sample (200-1000 μm thickness). The diffuse reflectance (R_d) is calculated: $R_d = R_t - r_{sp}$, where r_{sp} is the specular reflectance from the sample surface. **(c)** Example measurements of $T_{collimated}$, T_t, and R_d are shown for bloodless dermis

reflectance consists of the specular reflectance, r_{sp}, off the front air/tissue interface and diffuse reflectance, R_d, of photons by the tissue: $R_t = r_{sp} + R_d$. The measurements of T_t and R_d are then used to deduce the absorption, μ_a, and effective scattering, $\mu_s(1-g)$, coefficients of the tissue.

The sphere is hollow with an interior wall that is diffusely reflective, for example our sphere was covered with a layer of $BaSO_4$ with ~98% reflectivity. Tissue samples are held between glass slides during measurements, and thicknesses measured by micrometer. The tissue sample is first placed at the front port and collimated light is delivered to the sample from outside the sphere. Transmitted light, T_t, is captured by the sphere and undergoes multiple reflections off the sphere wall. A detector at another port views one side wall and collects a sample of the light within the sphere. A reference beam of light is delivered through a second port and strikes the wall. The measurement of the sample, M_{sample}, is normalized by the reference measurement of the wall, M_{wall}. Both measurements are made with the sample in place, therefore the throughput efficiency of the sphere is constant (a lossy tissue sample will lower the throughput efficiency of a sphere). The final transmittance is calculated: $T_t = (M_{sample}/M_{wall})$. To measure R_t, the sample is placed at the rear port and the beam enters the front port to strike the sample from the sphere interior. Reflected light is captured by the sphere. Similar measurements of M_{sample} and M_{wall} are made, and the diffuse reflectance is calculated: $R_d = (M_{sample}/M_{wall})(0.98) - r_{sp}$, where r_{sp} is calculated for the air/glass/tissue interface to be 0.051 (refractive indices of 1/1.54/1.37, respectively).

The R_d measurement is required rather than the R_t measurement because the R_d involves light that has penetrated into the tissue and sampled its optical properties. Specular reflectance (r_{sp}) has no information about the tissue interior. In our experiments, the sphere was aligned to collect r_{sp}, therefore R_t was measured. We determined $R_d = R_t - r_{sp}$, after calculating the r_{sp} from the air/glass/tissue interface.

Figure 2c illustrates typical measurements of R_d and T_t using an integrating sphere for a tissue sample of 360-μm thickness, from Prahl [4].

3.2.3 Analysis of data

The analysis involves three measurements, $T_{collimated}$, T_t, and R_d, to deduce three unknown optical properties: μ_a, μ_s, and g. The tissue thickness for the experiments must also be known.

The analysis of integrating sphere measurements of R_d and T_t to yield μ_a and $\mu_s(1-g)$ requires the use of a theory for optical transport. In these experiments, a version of diffusion theory was employed (Jacques and Prahl, 1987 [5]; Prahl, 1989 [4]). An iterative algorithm progressively converges onto a pair of μ_a and $\mu_s(1-g)$ values which yield predicted R_d and T_t values that best match the experimental measurements.

The total attenuation experiments yielded a single $T_{collimated}$ value that specifies a single value for the sum $(\mu_a + \mu_s)$, see eq. 5. Combining this $(\mu_a + \mu_s)$ value with the μ_a and $\mu_s(1-g)$ values from the integrating sphere experiment allows specification of all three optical properties: μ_a, μ_s, and g.

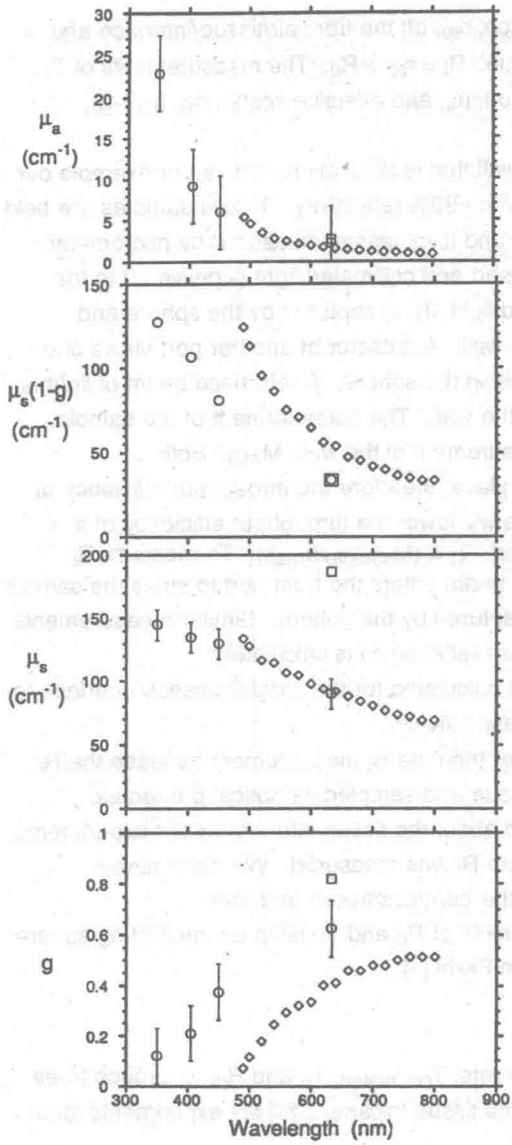

Figure 3: Optical properties of bloodless dermis.
The absorption coefficient, μ_a, and reduced scattering coefficient, $\mu_s(1 - g)$ were deduced from integrating sphere measurements of R_d and T_t. The sum ($\mu_s + \mu_a$) was specified by total attentuation measurements of $T_{collimated}$, which primarily specifies μ_s since $\mu_s >> \mu_a$. The anisotropy, g, was deduced from the μ_a, $\mu_s(1 - g)$ and ($\mu_s + \mu_a$) values. (Circles: Zrakit [3]. Diamonds: Prahl [4]. Box: Jacques et al. [2].)

3.2.4 Optical properties of bloodless dermis

The optical properties of bloodless dermis at about 85% water content are summarized in Fig. 3. The data of Zrakit (circles) show standard deviations for 30 samples. The data of Prahl (diamonds) are for a single sample. The 633-nm wavelength data of Jacques et al. (box) are based on samples from five subjects.

The absorption coefficient, μ_a, and the effective scattering coefficient, $\mu_s(1-g)$, were determined by the integrating sphere measurements. The absorption coefficient, μ_a, is shown in Fig. 3a, and increases dramatically for shorter wavelengths below 500 nm. The effective scattering coefficient, $\mu_s(1-g)$, is shown in Fig. 6b and decreases with increasing wavelength.

The total attenuation data yields the sum ($\mu_a + \mu_s$), which is dominated by the μ_s value, and allows $\mu_s(1-g)$ to be separated into its component factors, the scattering coefficient, μ_s, (Fig. 6c) and the anisotropy, g, (Fig. 6d). The μ_s value decreases with increasing wavelength more slowly than does $\mu_s(1-g)$. The g value increases with longer wavelength.

Some comments on the variation in data: Figures 6a and b indicate relatively good agreement of three sets of integrating sphere data at 633 nm. However, the total attenuation experiments differed. The measurements of Jacques et al. [2] used a HeNe laser beam rather than the spectrophotometer beam of the Zrakit and Prahl measurements. The HeNe laser beam may have allowed a more rigorously collimated measurement. For whatever reason, the ($\mu_a + \mu_s$) value of Jacques et al. was greater (~190 cm^{-1}) than the spectrophotometer measurements of the Zrakit and Prahl (~92 cm^{-1}). Therefore, the μ_s value (box) in Fig. 6c is greater, and the corresponding g value (box) in Fig. 6d is greater. It should be pointed out that the Jacques et al. g value of 0.82 from integrating sphere measurements matched the 0.81 g value based on their goniometry experiments [2]. Such self-consistency lends support to these measurements.

3.2.5 Light penetration into bloodless dermis

The discrepancies in optical properties stem principally from the technical difficulties inherent in the total attenuation experiments, which allow separate specification of μ_s and g. However, the deep penetration of light into tissue is dominated by the pair of optical properties, μ_a and $\mu_s(1-g)$. Therefore, the discrepancies do not strongly influence the prediction of deep light penetration. The penetration depth (∂) is often cited to characterize light penetration, and is defined:

$$\partial = \frac{1}{\sqrt{3\mu_a(\mu_a + \mu_s(1-g))}} \qquad (6)$$

The expression for fluence rate (ϕ in W/cm^2) versus depth (z) can be approximated:

$$\phi(z) = \phi_o \, k \, e^{-z/\partial} \qquad (7)$$

where ϕ_o is the delivered irradiance (W/cm^2) and k is a scalar that accounts for the augmentation of surface ϕ due to backscattered light. This approximate expression is only accurate away from the surface, at depths $z>\partial$.

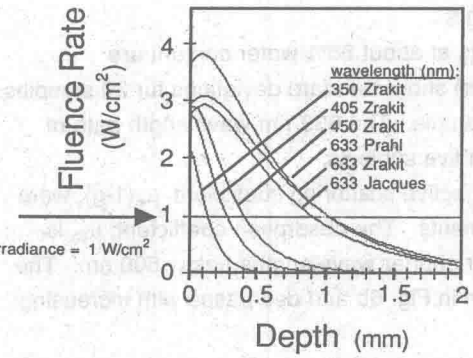

Figure 4: Optical penetration into bloodless dermis.
The light distribution within bloodless dermis is plotted as fluence rate versus depth, using the delta-Eddington diffusion approximation [4], for an irradiance of 1 W/cm^2. The distribution of several wavelengths are presented, based on the optical properties of Zrakit [3] (see Fig. 3). For 633 nm, the light distributions are calculated from the data of Zrakit [3], Prahl [4], and Jacques et al. [2] for comparison. Despite discrepancies in optical properties, all three data sets yield similar light penetration.

In Fig. 4, the light distribution, $\phi(z)$, in bloodless dermis is shown for several wavelengths. Longer wavelengths penetrate deeper into the dermis. The amount of light near the surface is 2-3 fold greater than the delivered irradiance (ϕ_o = 1 W/cm^2), due to the augmentation of irradiance by backscattered light. Note that the $\phi(z)$ calculated using the three sets of optical properties at 633 nm (Zrakit, Prahl, and Jacques et al.) are shown to allow comparison. Despite the discrepancies in optical properties, all three curves shown similar light penetration into skin. Only near the tissue surface is there disagreement.

3.3 Pigmented epidermis: *In vivo* optical fiber reflectance spectroscopy

The optical properties of the epidermis are not much different from those of dermis [6]. Moreover, because of the very thin thickness of the epidermis (60-100 μm) the slight error in approximating epidermal properties by dermal properties is not significant. However, one aspect of epidermal optics is very dominant: melanin absorption. The variation in melanin content from subject to subject is quite significant. Therefore, some attempt to document the absorption spectrum of epidermal melanin *in situ* is needed. Then it is possible to add any desired amount of melanin to the epidermis in a model computer simulation of skin optics.

To accomplish this task, *in vivo* measurements of reflectance were made on normally pigmented versus vitiligo skin sites on the forearm of a Caucasian human volunteer using an optical fiber reflectance spectrophotometer. The system delivers white light from a tungsten-halogen lamp source through one arm of a bifurcated optical fiber bundle, and collects light with the other arm. At the terminus, the two arms are randomly

mixed to yield a mixed-fiber bundle that contacts the skin. The collected light is carried to a diode-array spectrophotometer for detection. The system was calibrated by a measurement of a standard material (Spectralon™; Labsphere, Inc., New Hampshire, USA; $R_{std} \approx 0.994$ over visible spectrum).

The reflectance measurement is very similar to a transmission measurement through a cuvette in a spectrophotometer. The pathlength of light, L, is well-defined in a cuvette of clear solution (eg., L = 1 cm), and the transmission is dependent on the extinction coefficient, ε, and concentration, C, of absorber in the solution: $T = 10^{-\varepsilon CL} = 10^{-OD}$. The OD refers to the *optical density* of the solution. But L is not known in a turbid tissue such as skin since photons scatter over a range of pathlengths before escaping as reflectance. Nevertheless, the reflectance can be expressed: $R = 10^{-OD}$ where OD is the apparent optical density of the skin:

$$OD = -\log_{10}(R) \tag{8}$$

In practice, it is necessary to calibrate a reflectance spectrophotometer. The light delivery system provides a source term (S) that varies with wavelength. The detector system has a wavelength-dependent response (D). The fraction (f) of reflected light that is successfully collected by the optical fiber bundle that contacts the skin (or the standard material) is affected by loss of light due to lateral light diffusion in the turbid tissue, which is wavelength dependent. Skin reflectance spectrum measurements (M_{skin}) were normalized by the spectral measurement of the standard (M_{std}). Therefore, the data was recorded as:

$$\frac{M_{skin}}{M_{std}} = \frac{SDR_{skin} f_{skin}}{SDR_{std} f_{std}} = R_{skin} f^* \quad \text{where } f^* = \frac{f_{skin}}{R_{std} f_{std}} \tag{9}$$

The term f^* is somewhat close to unity in value, but can vary with wavelength (this paper will not discuss the experimental specification of f^*). In Figure 5, the optical density spectra of skin at the normally pigmented and vitiligo sites are plotted as $-\log_{10}(R_{skin} f^*)$ versus wavelength. The difference spectra, $OD_{normal} - OD_{vitiligo} = -\log_{10}(R_{normal} f^* / R_{vitiligo} f^*)$, is also plotted. The term f^* cancels in the difference spectrum, therefore the difference spectrum is reliably attributed to the epidermal melanin without calibration artifact.

The absolute value of the epidermal melanin content can be characterized by the spectrophotometer measurements. Kollias and Baqer [7,8] reported that the magnitude of the slope of the OD versus wavelength in the spectral range 620-720 nm is directly proportional to the quantity of melanin in the epidermis. The more melanin, the steeper is the negative slope of OD versus wavelength (units of nm^{-1}). To illustrate this observation in a nonbiological solution, Kollias and Baqer measured transmission through a solution of DOPA-melanin, created by exposure of L-DOPA to sunlight which polymerizes the molecules into a synthetic melanin polymer that is similar to epidermal melanin in its long-wavelength spectrum [8]. Plotting optical density (OD) versus wavelength, the straight lines through the 620-720 nm data for five solutions of DOPA-melanin had different slopes between 620-720 nm which were proportional to the mg/ml concentration of DOPA-